RSC Advances

PAPER

View Article Online
View Journal | View Issue

Cite this: *RSC Adv.*, 2021, **11**, 34355

Supported Pt–Cu bimetallic catalysts: preparation and synergic effects in their catalytic oxidative degradation of aniline†

Qiuyue Ding,‡[a] Wumin Zhang,‡[a] Yuanyuan Zhu,[b] Lu Wang,[b] Xinyuan Feng,[b] Yanyan Xi[bc] and Xufeng Lin*[ac]

Catalytic Fenton oxidation is an effective way to remove organic pollutants in water, and the performance of the catalyst is a key issue for the competiveness of this method. In this work, various supported bimetallic Pt–Cu catalysts were prepared by different impregnation methods and their performances for catalytic Fenton oxidation of aniline in water were investigated. In the different impregnation methods employed, factors including the reduction method of the metal precursor, type of catalytic support, and loading of metal were investigated. The effect of different reduction methods on actual loadings of the active components on the supported Pt–Cu catalysts showed the order of (i) H_2 reduction > (ii) liquid phase methanal reduction. Meanwhile, compared with the monometallic catalysts, the Pt–Cu alloy phase (mainly in the form of $PtCu_3$) was generated and the specific surface area was significantly reduced for the bimetallic catalysts. In the process of Fenton catalytic oxidation of aniline, it was found that most of the prepared catalysts had a certain catalytic activity for H_2O_2 accompanied with aniline degradation. It was found that $Pt_{0.5}Cu_{1.5}$/AC (where AC denotes activated carbon) exhibited superb catalytic activity compared with all other prepared catalysts. In particular, aniline was almost completely mineralized in a neutral solution (500 mg L^{-1} aniline, 0.098 mol L^{-1} H_2O_2) after 60 min at 50 °C using Pt–Cu/AC (Pt: 0.5%, Cu: 1.5%). The characterization results showed that the Pt and Cu components were rather evenly distributed on the AC support for this catalyst. More importantly, there was an obvious synergic effect on the supported bimetallic catalyst between the Pt and Cu components for the catalytic oxidation of aniline.

Received 29th July 2021
Accepted 15th October 2021

DOI: 10.1039/d1ra05762f

rsc.li/rsc-advances

1. Introduction

In recent years, environmental accidents caused by aniline pollution[1] have frequently occurred, and thus the treatment of aniline wastewater has become a hot topic in the research field of water treatment.[2,3] The development of economical, environmentally friendly and efficient treatment technologies are undoubtedly always desirable for disposal of waste water in general and of that containing aniline in particular.[4] In general, the treatment technologies for wastewater containing organic pollutants have a long history of research and practice, and they can be roughly classified into physical, chemical and biochemical methods.[5,6] The traditional physical and biochemical treatment methods always require a rather long time to degrade organic compounds in wastewater. Owing to its fast speed and ability to achieve rather complete degradation of organic pollutants, chemical treatment method casts more and more attentions,[7] like incineration,[8] chemical oxidation,[9] advanced oxidation processes (AOPs).[10] AOPs including Fenton oxidation, catalytic-ozone oxidation and photocatalytic oxidation,[11–14] share a general principle that highly-active oxygenated intermediate like ˙OH radicals are generated to oxidize the organic pollutants efficiently and thoroughly.[15–17] In particular, Fenton oxidation method is suitable for degrading a variety of non-biodegradable organic substances.[18,19] However, the traditional Fenton oxidation method suffers from the following problems, such as requiring a low aqueous pH value (typically around 3), the presence of a large amount of metal ions in the treated solution leading to a second-time contamination, insufficient amount of ˙OH produced, and poor catalytic activity, *etc.*[20–22]

To overcome the above-mentioned problems, various types of new supported metal catalysts were developed, in particular, transition metals components like Fe and Cu immobilized on porous catalytic supports. For example, Stair *et al.*[23] loaded Cu onto carbon microspheres using a spray-drying method, and

[a]*Department of Chemistry, College of Science, China University of Petroleum (East China), Qingdao, 266580, P. R. China. E-mail: hatrick2009@upc.edu.cn*

[b]*College of Chemical Engineering, China University of Petroleum (East China), Qingdao, 266580, P. R. China*

[c]*State Key Laboratory of Heavy Oil, China University of Petroleum (East China), Qingdao, 266580, P. R. China*

† Electronic supplementary information (ESI) available. See DOI: 10.1039/d1ra05762f

‡ These authors contributed equally to this paper.

the obtained catalysts presented excellent performance for the Fenton oxidative degradation of methyl orange, methyl blue, and rhodamine B in aqueous solutions. Yao *et al.*[24] reported that FeO_x/SiO_2 catalyst could degrade aniline to a low concentration (1 mmol L^{-1}). In addition, the conversion of aniline was 79% at pH = 3 and at the temperature of 30 °C after 160 min of reaction. In whole, novel supported metal catalysts have good potentials for degradation as well as mineralization of refractory organic pollutants. Researches on supported bimetallic Fenton-like systems are being carried out by using one metal catalyst after another, and currently there are only a few researches focusing on bi-transition metallic catalysts. For example, Choi *et al.*[25] used Fe/Al as a heterogeneous Fenton catalyst for the oxidation of acetone, achieving an acetone conversion rate of up to 78.5%. The reason for the high conversion is that different metal ions may show a synergic catalytic effect in the bimetallic multi-type Fenton system.[26] At the same time, it has a certain effect on suppressing the dissolution of catalytic metal ions.[27] However, the researches focusing on the supported catalysts containing one noble metal component and another transition metal component are sparse. As is known, supported bimetallic catalysts containing precious metals often show good synergistic effects for reactions other than Fenton oxidation even though the metal loadings were extremely low.[28] For instance, synergy between Pt and Re was found in carbon-supported Pt, Re, and Pt–Re catalysts, which were used in aqueous phase reforming (APR) of glycerol and water gas shift (WGS) reactions.[29]

In order to degrade high concentration of aniline in water, various strategies have been adopted to improve the activity of heterogeneous Fenton catalysts. For example, Liu *et al.*[30] reported that Ni–Fe oxalic acid complex catalyst (the total loadings of Ni + Fe being about 31%) was used for the degradation of 20 mg L^{-1} aniline. The removal efficiency of aniline was ~100% at pH = 5.4 after a 35 minute reaction, and the total organic carbon (TOC) removal rate was 88%. According to report in the literature,[31–34] other metal components can be added to modify the supported precious metal catalysts. For example, Xie *et al.* found that the interaction of Pt and other metals was beneficial for improving the exposure rate of Pt nanoparticles on catalytic supports. The low-temperature reduction method could also prevent the high-temperature agglomeration of Pt particles.[34]

This work aims at providing new supported bimetallic catalyst for improved efficiency for Fenton oxidation of high-concentration aniline in water. Since both of Pt and Cu are often used in catalytic oxidation of organic compounds,[35–38] these two metal elements were selected in this work to prepared supported bimetallic catalysts, partly for understanding whether they can present a synergic effect for Fenton oxidation of aniline. From the aspect of catalyst preparation method, the equal volume impregnation method[39,40] under different conditions (including different types of catalytic support, amounts of metal loading and reduction methods) were examined. By developing new reduction method other than hydrogen reduction, highly dispersed metal components can be obtained on the catalyst surface, which can be beneficial to aniline oxidation. To the best of our knowledge, the preparation of supported Pt catalyst using imidazolidinyl urea as reductant, and the Pt-based supported bimetallic catalyst used for the oxidative degradation of aniline were both reported for the first time. The catalytic results reported in this work provide a potentially hopeful method for efficient removal of aniline pollutant in water.

2. Experimental section

2.1 Materials

Chloroplatinic acid ($H_2PtCl_6 \cdot 6H_2O$, AR, Pt > 37.5%), copper nitrate ($Cu(NO_3)_2 \cdot 3H_2O$, AR, 99%), iron nitrate ($Fe(NO_3)_3 \cdot 9H_2O$, AR), methanal (CH_2O, AR), potassium permanganate ($KMnO_4$, ≥99.5%), sodium hydroxide (NaOH, ≥96%), and aqueous hydrogen peroxide solution (H_2O_2, AR, H_2O_2 being 30 wt%) were provided by Sinopharm Chemical Reagent Co, Ltd. Imidazolidinyl urea ($C_{11}H_{16}N_8O_8$, AR, 98%) was provided by Aladdin Reagent (Shanghai) Co, Ltd. Alumina (Al_2O_3) particles were provided by Yantai Henghui Chemical Co, Ltd. SiO_2 (20–40 mesh) particles were provided by Qingdao Ocean Chemical. Activated carbon (20–40 mesh) was provided by FuJian Xinsen Carbon Co, Ltd. All chemicals were of analytical purity and used without further treatment. Deionized (DI) water was applied for the whole experiment.

2.2 Catalyst preparation

Supported Pt–Cu catalysts were synthesized using an equal volume impregnation method with the following steps, and the routine procedures can be found elsewhere in the literature.[35] As a typical example, the preparation procedure of a $Pt_{1.5}Cu_{0.5}/Al_2O_3$ (the subscripts of 1.5 and 0.5 representing roughly the weight percents of Pt and Cu, respectively) catalyst containing 5 steps is described as follows.

First, 4.0 g Al_2O_3 (being 20–40 mesh particles) was placed in a crucible, transferred into a muffle furnace and heated to 500 °C in air for 4 h to remove moisture and organic impurities. The calcined Al_2O_3 particles were placed in a clean plastic ziplock bag after cooling down. This step can be named as a precalcination step.

The second step was to impregnate the Cu component into Al_2O_3. For each gram of precalcined Al_2O_3, $Cu(NO_3)_2 \cdot 3H_2O$ of 0.0193 g was dissolved in 0.90 g DI water, and the obtained Cu(II) solution was mixed with the Al_2O_3 particles. It should be noted that the volume of water in above the Cu(II) solution was equal to the water absorbed by amount of the calcined Al_2O_3 (0.90 g water can be absorbed by per gram of Al_2O_3).

In the third step of metal component reduction, Al_2O_3 particles impregnated with the Cu components were kept at room temperature for 12 hours and then were treated in a H_2 flow at 300 °C for 4 h in order to reduce the Cu components. At this stage, the obtained sample can be named as $Cu_{0.5}/Al_2O_3$.

The fourth step was to impregnate the Pt component to $Cu_{0.5}/Al_2O_3$, which was similar to the second step, with the only differences in that 0.0406 g $H_2PtCl_6 \cdot 6H_2O$ took the place of 0.0193 g $Cu(NO_3)_2 \cdot 3H_2O$.

The fifth step was to reduce the Pt component, and the treatment process was almost the same to the third step of Cu-

component reduction. Finally, the catalyst obtained by these steps was represented as $Pt_{1.5}Cu_{0.5}/Al_2O_3$, where the percentages, indicated in the subscripts in the catalyst notation, were calculated from the mass of the Pt or Cu element relative to that of the Al_2O_3 support.

Different from the above-mentioned procedure (called standard preparation procedure), one or more of the preparation conditions including impregnation amount, bimetallic type, impregnation ratio of two metals, reduction temperature, reduction method, and type of catalytic support were changed to obtain different catalysts. These preparation methods are described as follows by comparing with the above-described standard preparation procedures.

For Pt_nCu_m/Al_2O_3 catalyst: change the amount of Cu and Pt sources in steps 2 and 4, respectively, to obtain the target weight percent of n% and m%, where $(n + m)$ was always kept at 2.0. The detailed n and n value will be specified in the text hereafter.

For Pt_nCu_m/Al_2O_3-600 catalysts: compared to the case of Pt_nCu_m/Al_2O_3, the H_2 treatment temperature was 600 °C instead of 300 °C in steps 3 & 5.

For Pt_nCu_m/SiO_2 catalysts: use SiO_2 instead of Al_2O_3 particle as catalytic support.

For Pt_nFe_m/Al_2O_3 catalysts: use $Fe(NO_3)_3 \cdot 9H_2O$ instead of $Cu(NO_3)_3 \cdot 3H_2O$ in the second step in order to impregnate the Fe component into the catalytic support.

For Pt_nCu_m/AC catalysts: use activated carbon instead of Al_2O_3 particle as the catalytic support, and the pre-calcination temperature was 300 °C in step 1.

For Pt_nCu_m/AC-MR catalysts: compared to the case of Pt_nCu_m/AC, in the fifth step, methanal reduction (MR) method was developed in this work. The Pt component impregnated AC particles was reduced at 80 °C in a solution containing imidazolidinyl urea having the same number of mole as the Pt source, excess amount of methanal, and having a pH value of 11. Then the particles were washed with a large amount of water and then dried at 120 °C over night. The reduction method will be named as methanal reduction method hereafter.

2.3 Catalyst characterization

The crystal phase structure of supported metal catalysts was measured by a powder X-ray diffractometer (XRD, D8 Advance, Germany) using a Cu K_α radiation (λ = 0.15418 nm) having a power of 2.2 kW with a scanning step of 0.02° and a 2θ range of 2–75°.

In a temperature-programmed reduction by H_2 (H_2-TPR) measurement of a certain catalyst, the H_2 signal was monitored by a thermal conductivity detector (TCD). First, the catalyst was pre-treated for a period of time (~30 min) in an Ar flow, then switched to a 20 sccm flow of 10% H_2–He for 20 min after cooling down to room temperature, and then heated up to 800 °C at a rate of 10 °C min^{-1}. The TCD pool was kept at 60 °C & 30 mA.

Scanning electron microscope (SEM) and energy spectrometer (SEM-EDX) were used to analyze the morphology of the sample, and the element distribution by mapping. The working voltage of the instrument was 10.0 kV, the solid sample was more than 10 mg and needed to be dried and processed. Transmission electron microscopy (TEM) projected an accelerated and concentrated electron beam onto a very thin sample to collide, resulting in solid angle scattering, and get an image of light and dark. It was used to observe the morphology and dispersion of nanoparticles and measure the particle size of nanoparticles.

The N_2 adsorption–desorption curves of samples were obtained by specific surface area and microporous physical adsorption analysis. Brunauer–Emmett–Teller (BET), Barret–Joyner–Halenda (BJH) were used to calculate the specific surface area and pore size distribution.

Thermogravimetric (TG) analyzed the decomposition temperature of samples. TG experiments were carried out in N_2 flow (60 mL min^{-1}), and heated from 40 °C to 800 °C at a heating rate of 10 °C min^{-1}.

The prepared catalysts were ground to >200 mesh particles and then X-ray fluorescence (XRF, PANalytical, Netherlands) spectroscopy was used to measure the Si, Al, Pt or Cu contents of the catalysts.

2.4 Catalytic Fenton oxidation of aniline

The Fenton oxidation of aniline was performed in a 250 mL flask equipped with a water bath thermostat as the reactor. In a typical oxidation experiment, a 200 mL aniline aqueous solution (500 mg L^{-1}) was added to the reactor. The temperature of the reaction system was heated to 50 °C by a water bath, and then a 2.0 mL H_2O_2 solution (30 wt%) was added to the above aniline solution (thus the concentration of H_2O_2 being 0.087 mol L^{-1} at the beginning of the reaction). At the absence of a catalyst, it was confirmed that there was no observable reaction between H_2O_2 and aniline at the reaction temperature. Then 1.0 g selected catalyst (or 5.0 g_{cat} L_{water}^{-1}) was added to the reactor in order to initiate the catalytic oxidation reaction.

A 2.0 mL liquid was sampled from the reaction mixture at certain time intervals, and then centrifuged to separate solid residue. The liquid sample was then analyzed by a HACH DR 1010 chemical oxygen demand (COD) analyzer or a TOC-LCPH/CPN total organic carbon content (TOC) analyzer. The catalytic performance of a certain catalyst was evaluated by calculating the COD or TOC removal rate of the reaction mixture where the catalyst was used.

2.5 Catalytic decomposition of H_2O_2

The catalytic H_2O_2 decomposition was performed with the same reaction conditions mentioned above (Section 2.4), with the only difference in that the 500 mg L^{-1} aniline solution was replaced by DI water of a same volume.

At a certain reaction time, a 2 mL sampled solution was mixed with a 2 mL 3 mol L^{-1} sulfuric acid. The concentration of H_2O_2 was determined by acidic $KMnO_4$ (5 mol L^{-1}) titration, according to the volume of $KMnO_4$ solution consumed. The titration reaction principle[41] can be expressed as follows:

$$2MnO_4^- + 5H_2O_2 + 6H^+ \rightarrow 2Mn^{2+} + 5O_2 + 8H_2O$$

Table 1 The actual Pt and Cu loadings of the Pt–Cu/AC catalysts measured by XRF spectroscopy. See Section 2.2 for catalyst preparation procedure as well

Catalyst	Pt wt%	Cu wt%
$Pt_{1.5}Cu_{0.5}$/AC-MR	1.329	0.386
$Pt_{1.0}Cu_{1.0}$/AC-MR	0.894	0.775
$Pt_{0.5}Cu_{1.5}$/AC-MR	0.445	1.275
$Pt_{1.5}Cu_{0.5}$/AC	1.529	0.446
$Pt_{1.0}Cu_{1.0}$/AC	0.994	0.965
$Pt_{0.5}Cu_{1.5}$/AC	0.505	1.475

3. Results and discussion

3.1 Results about the novel preparation method of the Pt–Cu/AC bimetal catalysts

It is noticeable that the impregnation and metal component reduction methods for preparing the Pt–Cu/AC catalysts (see Section 2.2 for detail) is reported for the first time. The main motivation for us to develop a new liquid phase reduction method came from the case that the activated carbon (AC) support may tend to be damaged at high temperatures. In addition, treatment with imidazolium urea solution before reduction can decrease the risk of agglomeration of metal nanoparticles at high temperatures, which could make the Pt and Cu active components more uniformly dispersed on the catalytic supports. This hypothesis was further verified by the TEM images of catalyst as shown later in this paper.

Table 1 shows that the metal content losses of the Pt–Cu/AC catalysts prepared with the methanal reduction (MR) method were higher than those prepared with the H_2 reduction method. The Pt and Cu loading rates (loading rate = actual loading/theoretical loading calculated from the experimental conditions) in the former case were about 88% and 77%, respectively, which are close to 100% for the latter case. Possible reasons accounted for this phenomenon could be as follows. (i) The times for ultrasonication during impregnation and liquid phase reduction were insufficient. (ii) The pores of catalytic supports became narrower after the first impregnation and reduction steps, which hindered the loading of the second metal component.

3.2 Catalyst characterization results for physiochemical properties of catalysts

The H_2-TPR profiles presented in Fig. 1a shows that the reduction temperature of the unreduced $Cu_{2.0}/Al_2O_3$ catalyst started from ~380 °C with the peak around ~600 °C. The curves in Fig. 1b and c indicate that the metal components on the prepared supported Cu and Pt/Al_2O_3 catalysts was reduced to their metallic states. Xi *et al.* had reported that the reduction conditions of the 2% Pt/Al_2O_3 catalyst[35] reduced in presence of H_2 at 300 °C for 4 h, which is consistent in the results in Fig. 1c.

Fig. 2 shows the XRD patterns of some selected catalysts. Inspection of Fig. 2a shows that, compared with the data of the reported standard XRD pattern in Table 2,[42–47] both curves (i) and (ii) were correspond to the characteristic peaks of γ-Al_2O_3. Therefore the main crystal phase of the catalytic supports after calcination was γ-Al_2O_3. Compared with Fig. 2c, it was found that the peaks of catalyst were changed from sharp to broad, showing that Al_2O_3 in the catalyst was amorphous alumina. Comparing between pictorial panels Fig. 2a and b, it can be seen that the catalysts with different reduction temperatures had different peak area and width, but the other characteristic peak positions were basically the same. Combined with the H_2-TPR results in Fig. 1, it can be further illustrated that the reduction

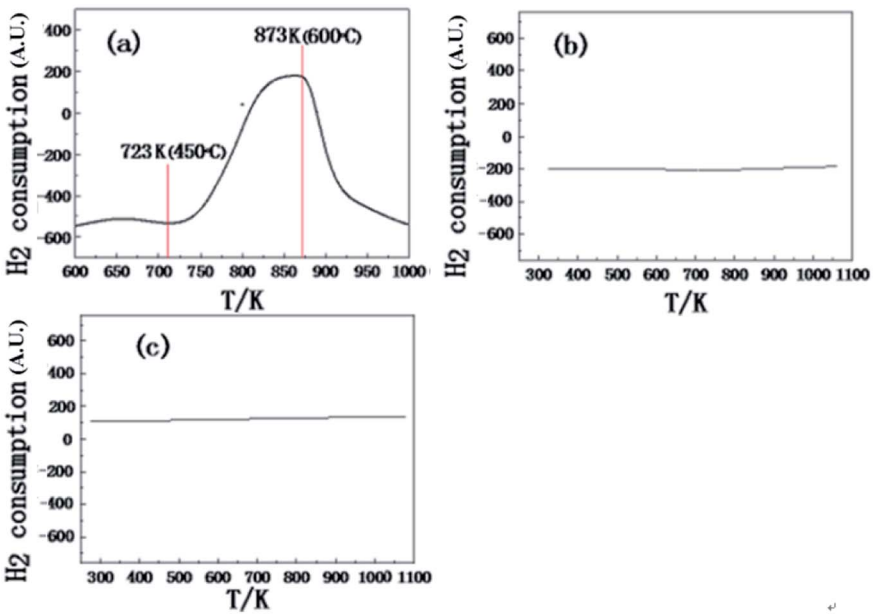

Fig. 1 The H_2-TPR profiles of the (a) $Cu_{2.0}/Al_2O_3$ (before H_2 reduction) (b) $Cu_{2.0}/Al_2O_3$ (after H_2 reduction) and (c) $Pt_{2.0}/Al_2O_3$ (after H_2 reduction) catalysts.

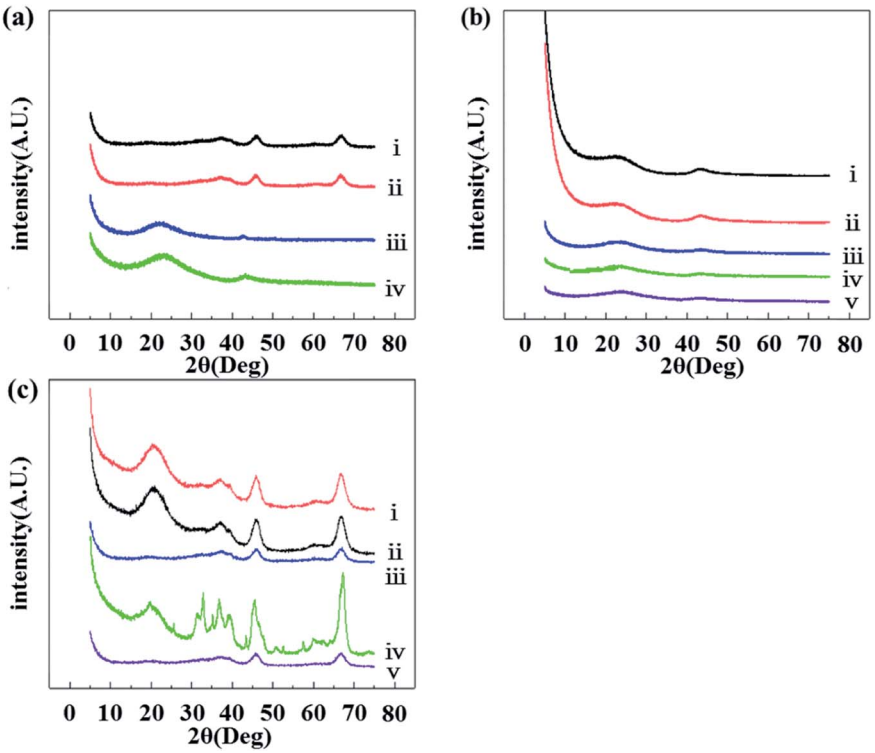

Fig. 2 XRD patterns of the prepared catalysts. In panel (a), curve (i): $Pt_{1.0}Cu_{1.0}/Al_2O_3$, (ii): $Pt_{1.0}Cu_{1.0}/Al_2O_3$-600, (iii): $Pt_{1.0}Cu_{1.0}/SiO_2$ and (iv): $Pt_{1.0}$-$Cu_{1.0}$/AC. In panel (b), curve (i): pure AC calcined at 300 °C for 4 h, (ii): uncalcined AC, (iii): $Pt_{1.5}Cu_{0.5}$/AC, (iv): $Pt_{1.0}Cu_{1.0}$/AC and (v): $Pt_{0.5}Cu_{1.5}$/AC. In panel (c), curve (i): $Pt_{1.5}Cu_{0.5}/Al_2O_3$, (ii): $Pt_{1.0}Cu_{1.0}/Al_2O_3$, (iii): $Pt_{0.5}Cu_{1.5}/Al_2O_3$, (iv): Al_2O_3 (calcined at 500 °Cfor 4 h), and (v): uncalcined Al_2O_3.

Table 2 The typical X-ray diffraction peak position[38–43] of AC, γ-Al_2O_3, Pt, Cu, Pt_1Cu_1, and Pt_1Cu_3

Peak position		1	2	3	4
γ-Al_2O_3	2θ/(°)	37.71	39.45	45.87	66.89
AC	2θ/(°)			43.92	51.28
Pt	2θ/(°)		39.79	46.28	67.53
Pt_1Cu_3	2θ/(°)			42.24	
Pt_1Cu_1	2θ/(°)			41.01	
Cu	2θ/(°)			43.30	

temperature had an effect on the complete reduction of Cu. For curves (ii), (iii), and (iv) in Fig. 2a, the matching characteristic diffraction peaks of Pt and Cu were not obvious. It also indirectly reflects that these components had low crystallinity. In combination with Table 2 which contains the standard peak positions of selected materials, a peak of the Pt–Cu compound indicating that a Pt–Cu alloy was formed, indicating that there was an interaction between the Pt and Cu components. Although the overall metal loadings for the cases of (ii), (iii) and (iv) in Fig. 2a were the same, the catalytic supports were different. Thus the width and area of the PtCu alloy peaks were different. This shows that the degree of the interactions between the Pt and Cu components were different, following the order of Pt–Cu/AC > Pt–Cu/SiO_2 > Pt–Cu/Al_2O_3. Fig. 2b shows that the peak width and intensity of the AC supports in the cases curve (i) and (ii) were basically unchanged before and after pre-calcination, indicating that the AC crystal phase did not have a noticeable change during calcination.

The N_2 adsorption–desorption isotherms, calculated BET surface area, average pore diameter and pore volumes of the prepared catalysts are shown in Fig. 3 and in Table 3. It can be noticed that the specific surface area of supports become larger after calcination, indicating that it was necessary to be pre-calcinated for the catalytic supports. As shown in Fig. 3, the nitrogen adsorption/desorption isotherms of the Pt–Cu catalysts on AC/Al_2O_3 and the calcined AC/Al_2O_3 supports belonged to the IUPAC IV and H1 type hysteresis loops, respectively. This shows that the catalytic materials were mainly mesoporous in structure and the pore size range was uniformly narrow.[48,49] The N_2 adsorption of the material becomes smaller after impregnation and metal reduction. The pore size of Pt–Cu/AC obtained from MR and the calcined supports was mainly between 2-4 nm, while the pore size of Pt–Cu/Al_2O_3 obtained from the H_2 reduction and the calcined Al_2O_3 was between 7–10 nm, as shown in Panels b, e and f in Fig. 3. This was due to AC has a greater specific surface area. The higher loading of Cu the catalyst had, the larger maximum pore diameter of the catalysts was, which may be related to the difference of particle size caused by incomplete reduction of Cu.

In general, the specific surface area of AC was increased from 1137 $m^2\ g^{-1}$ to 1415 $m^2\ g^{-1}$ after calcination at 300 °C for 4 h, while the pore volume and average diameter were unchanged. However the specific surface area of Al_2O_3 increased from 195

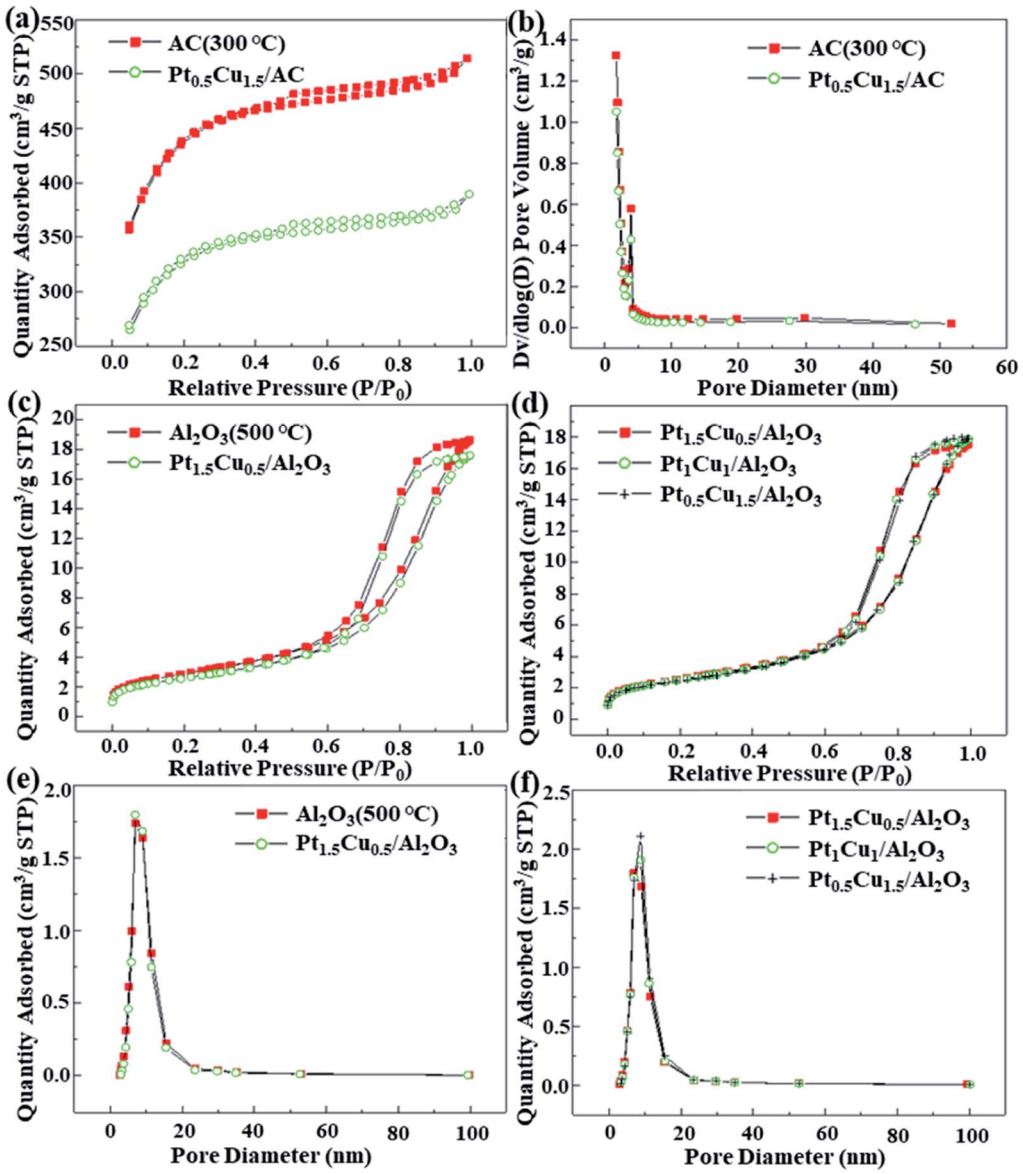

Fig. 3 N_2 adsorption–desorption isotherms and pore size distributions of selected catalysts as indicated in the figure. (a) Isotherms for pure AC and AC supported Pt–Cu catalyst. (b) Pore size distributions analyzed from (a). (c) and (d) Isotherms for pure Al_2O_3 and Al_2O_3 supported Pt–Cu catalysts. (e) and (f) Pore size distributions analyzed from (c) and (d), respectively.

$m^2\ g^{-1}$ to 228 $m^2\ g^{-1}$ after calcination at 500 °C for 4 h, and both of the pore volume and average diameter had a mild increase.

The pore volume and pore diameter of the catalysts with different supports obtained by the two-stage reduction had mild changes, reflecting that the platinum and copper entered the surface and the interior of the catalyst and changed the pore structure and specific surface area of the catalyst. While the difference between the specific surface area of the AC and Pt–Cu/AC was larger than the Al_2O_3 cases, indicating that AC was somehow destroyed at high temperatures. The specific surface area, pore volume and diameter of the supported Pt and Cu catalysts obtained from the methanal reduction changed little. The reason was that the specific surface area of AC was much larger than that of Al_2O_3 and SiO_2, and the pore volume and pore size are smaller than those of Al_2O_3 and this reduction method done little damage to the structural. Therefore, the Pt and Cu components were dispersed uniformly. For these catalysts, the order of specific surface area was: AC $\gg$ SiO_2 > Al_2O_3, and pore volume and pore size was: Al_2O_3 > AC > SiO_2. For Pt–Cu/Al_2O_3, when reduced at 300 °C and 600 °C in the H_2 atmosphere, the specific surface area was reduced from 202 $m^2\ g^{-1}$ to 192 $m^2\ g^{-1}$. The pore volume was basically unchanged, but the pore diameter was increased. This may be related to the reduction at high temperatures.

The TEM images of the selected catalysts are shown in Fig. 4. For the catalyst obtained from MR, the Pt particle size follows the order of $Pt_{1.0}Cu_{1.0}$/AC-MR > $Pt_{0.5}Cu_{1.5}$/AC-MR > $Pt_{1.5}Cu_{0.5}$/AC-MR > $Pt_{2.0}$/AC-MR. In all four cases the Pt or PtCu particles

Table 3 The specific surface area and pore size of the selected prepared catalysts in this work from their N_2 adsorption–desorption isotherms

Sample	Specific surface area S_{BET} ($m^2\ g^{-1}$)	Total pore volume ($cm^3\ g^{-1}$)	Average pore size (nm)
AC (uncalcined)	1137	0.29	2.74
AC (calcined at 300 °C, 4 h)	1415	0.30	2.71
$Pt_{1.5}Cu_{0.5}$/AC-MR	1030	0.25	2.72
$Pt_{1.0}Cu_{1.0}$/AC-MR	1029	0.24	2.74
$Pt_{0.5}Cu_{1.5}$/AC-MR	1028	0.23	2.76
$Pt_{0.5}Cu_{1.5}/Al_2O_3$	192	0.60	8.26
$Pt_{0.5}Cu_{1.5}/SiO_2$	437	0.14	2.56
Al_2O_3 (uncalcined)	195	0.57	7.50
Al_2O_3 (calcined at 500 °C, 4 h)	228	0.64	7.76
$Pt_{2.0}/Al_2O_3$	216	0.62	7.85
$Pt_{1.5}Cu_{0.5}/Al_2O_3$	205	0.62	7.83
$Pt_{1.0}Cu_{1.0}/Al_2O_3$	202	0.62	7.99
$Pt_{0.5}Cu_{1.5}/Al_2O_3$	202	0.61	8.05

were small and uniformly dispersed. The particle size of the Pt particles was in the range of 1–4 nm. In particular, the metal particle size of catalyst $Pt_{2.0}$/AC-MR mainly distributed in the 1–2 nm range, while those of Pt–Cu/AC catalysts presented a larger range of particle size mainly within 1–4 nm. This may be related to the formation of the Pt–Cu alloy, which made the metal particle size larger. In addition, the amount of Pt–Cu alloy with different loadings could be different, making the Pt particle size different.

The choice of catalytic support had a significant influence on the particle size of the active metal component for the catalysts with a same loading. The Pt particle sizes were in the range of 10–50 nm for $Pt_{0.5}Cu_{1.5}/Al_2O_3$, being much larger than those for the $Pt_{0.5}Cu_{1.5}/SiO_2$ case (2–8 nm). The Pt particle sizes were uneven for both cases, which was dramatically different to the Pt–Cu/AC cases. The Pt particle size distribution for the Al_2O_3 and SiO_2 cases was wide, which may be related to the nature of the support as well as the reduction method.

As can be seen in the following section about the results of catalytic reaction test, the $Pt_{0.5}Cu_{1.5}$/AC-MR catalyst presented desirably good catalytic performance. So, more characterization results focusing on the $Pt_{0.5}Cu_{1.5}$ catalysts were performed, with the results shown in the ESI† including the TG-DSC curves, SEM images and TEM-EDX elemental mappings.

3.3 Catalytic Fenton oxidation of aniline by H_2O_2

3.3.1 Effect of hydrogen peroxide concentration. Hydrogen peroxide is the direct source of reactive intermediates like $^{\bullet}OH$[50]

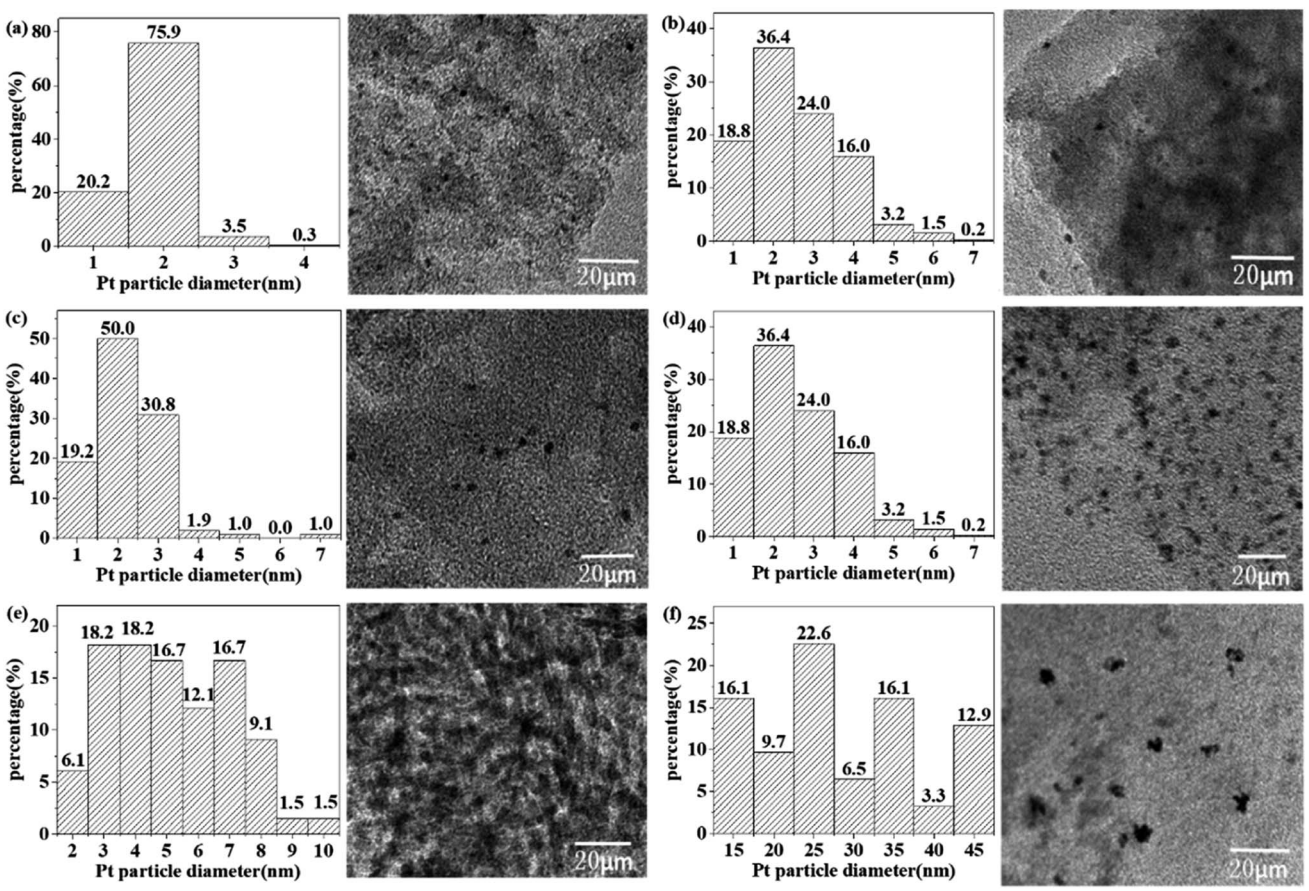

Fig. 4 The particle size charts and TEM images of (a) $Pt_{2.0}$/AC-MR, (b) $Pt_{0.5}Cu_{1.5}$/AC-MR, (c) $Pt_{1.0}Cu_{1.0}$/AC-MR, (d) $Pt_{1.5}Cu_{0.5}$/AC-MR, (e) $Pt_{0.5}Cu_{1.5}/SiO_2$ and (f) $Pt_{0.5}Cu_{1.5}/Al_2O_3$.

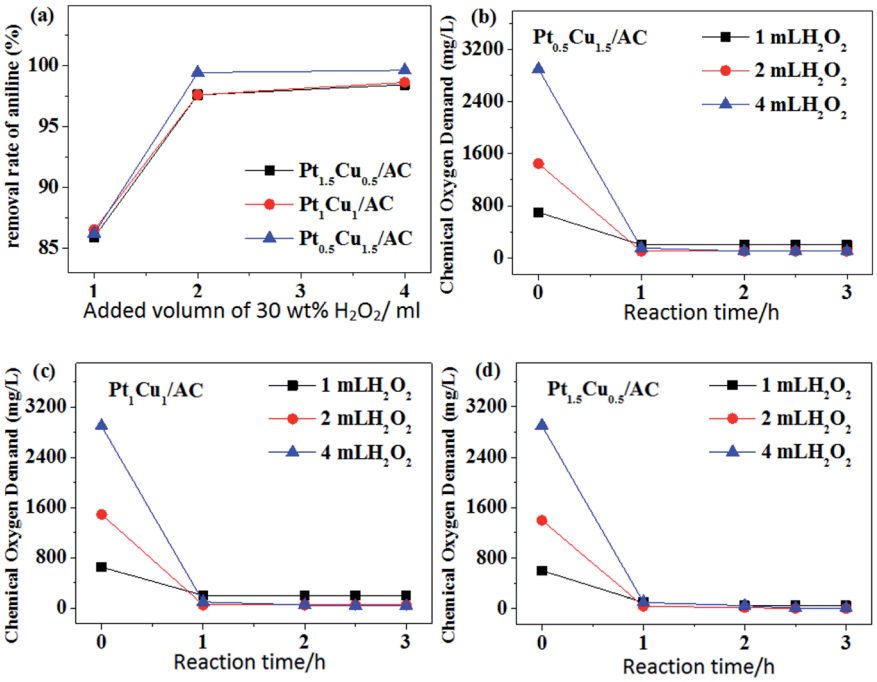

Fig. 5 Effects of different catalysts and H_2O_2 concentration on catalytic Fenton oxidation of aniline. (a) Effect of different Pt_nCu_m/AC-MR catalyst and H_2O_2 concentration on the removal of COD in the catalyzed oxidation of aniline after 3 h. (b) Effect of added volume of 30 wt% H_2O_2 to the reaction system on the removal of COD using the $Pt_{0.5}Cu_{1.5}$/AC-MR catalyst at different reaction times. (c) Effect of added volume of 30 wt% H_2O_2 to the reaction system on the removal of COD using the $Pt_{1.0}Cu_{1.0}$/AC-MR catalyst. (d) Effect of added volume of 30 wt% H_2O_2 to the reaction system on the removal of COD using the $Pt_{1.5}Cu_{0.5}$/AC-MR catalyst. *Reaction conditions: at the initial time of reaction, H_2O_2 concentration was 0.196, 0.098 and 0.049 mol L^{-1} with the added volume of 1.0, 2.0 and 4.0 mL, aniline concentration = 500 mg L^{-1}, catalyst dosage = 5 g L^{-1} temperature = 50 °C.

in the catalytic Fenton oxidation system in this paper. From Fig. 5a, it can be seen that the H_2O_2 concentration in the reaction system had an obvious influence on the catalytic degradation of aniline. For a same Pt–Cu/AC-MR catalyst, the COD removal rate follows the order 0.049 mol L^{-1} H_2O_2 (1 mL 30 wt% H_2O_2 added to the reaction system, see Section 2.4) $\ll$ 0.098 mol L^{-1} (2 mL) $\approx$ 0.196 mol L^{-1} (4 mL). For different Pt and Cu supported catalysts, the content of Pt, Cu and theirs alloys were different, resulting in different catalytic degradation effects of aniline (Fig. 5b–d).

When the amount of H_2O_2 was small, the amount of $^{\cdot}OH$ generated would be also small. On the other hand, the catalyst catalyzed the pure decomposition of H_2O_2 (see in Fig. 6), making the amount of $^{\cdot}OH$ effective for the catalytic oxidation of aniline further smaller. However, when the H_2O_2 concentration was too high, it also inhibited the production of $^{\cdot}OH$.[51] Therefore, there should be a most suitable H_2O_2 concentration for aniline degradation reaction system, which was 0.098 mol L^{-1} in this work.

The concentration of H_2O_2 had a great influence on the COD value, especially in the initial stage of reaction, and thus it also affected the apparent COD removal rate. It can be anticipated that H_2O_2 will also be decomposed catalytically in the presence of Pt–Cu catalysts, which intrigued us to test the performance of our prepared catalysts for pure decomposition of H_2O_2 at the absence of aniline in water.

It can be seen from Fig. 6 that for the Pt–Cu/Al_2O_3 catalysts the influence of the loading amounts of Pt and Cu components prepared under a same reduction method on the catalytic degradation of H_2O_2 was huge (panel a *vs.* b). When the loadings of Pt and Cu were fixed, the Pt–Cu bimetal catalysts with different supports carriers also had a great influence on the catalytic degradation of H_2O_2 (panel b *vs.* c). For all the Pt–Cu catalysts, the rate of catalytic decomposition of H_2O_2 always increased with the content of Pt. The decomposition rate of H_2O_2 was quite slow and basically unchanged after 30 minutes of reaction for all cases. This may be related to the rapid catalytic reaction caused by the high activity of Pt, which may also explain the rapid decrease of COD value during the degradation of aniline for 1 h in Fig. 5.

3.3.2 Effect of type of support. Since the value of COD cannot completely represent the conversion rate of aniline, the TOC value was also used for better evaluation. As can be seen from Fig. 7a, all catalysts prepared from three different catalytic supports had good catalytic performances. However, there was a certain deviation between the TOC removal rate of the catalysts prepared by Al_2O_3 and SiO_2 as supports with the order of SiO_2 > Al_2O_3. The TOC removal rate of Pt–Cu/AC-MR was the highest in three types of support, reaching above 97.5% (Fig. 7a). It was also found that the type of support and the reduction method had a great influence on removal rate of COD (Fig. 7c–e), with the order of COD removal rate of AC > SiO_2 > Al_2O_3 observed in this work. For three different Pt/Cu ratios on

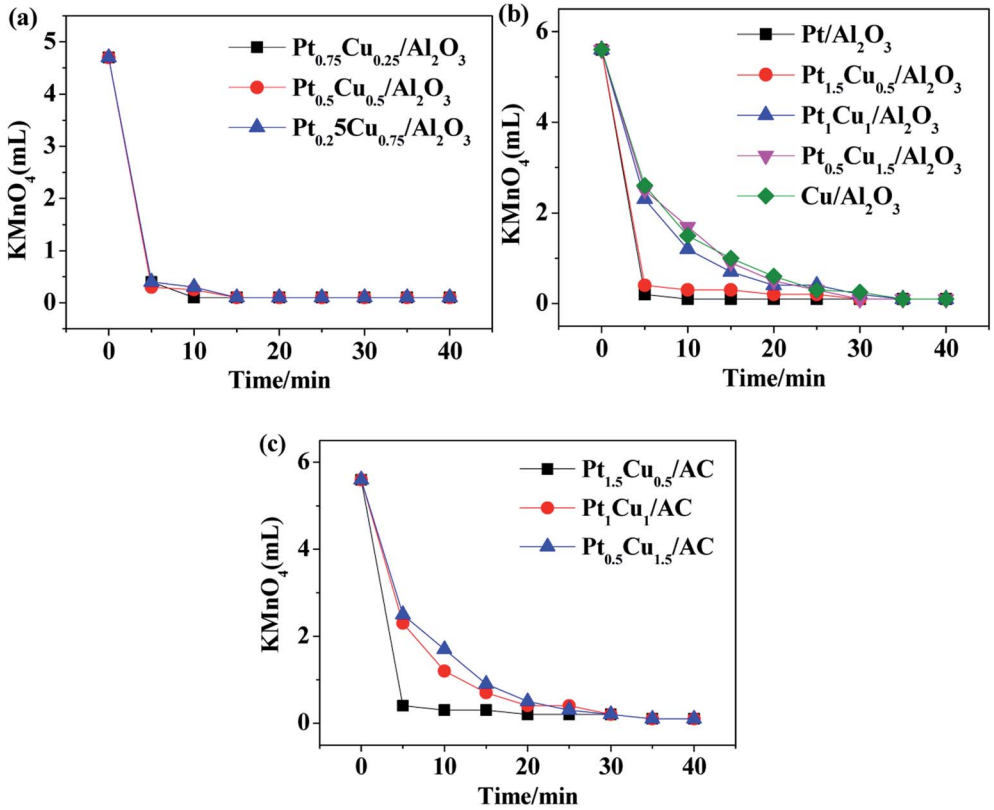

Fig. 6 H_2O_2 conversion in terms of volume of $KMnO_4$ consuming at the absence of aniline, at 50 °C and using 5 g L^{-1} of catalyst as indicated in the figure. See the experimental conditions in Section 2.5 in detail as well. (a) The Pt_nCu_m/Al_2O_3 catalysts, where $n\% + m\% = 1.0\%$, (b) the Pt_nCu_m/Al_2O_3 catalysts, where $n\% + m\% = 2.0\%$, (c) the Pt_nCu_m/AC-MR catalysts, where $n\% + m\% = 2.0\%$.

the Pt–Cu/AC catalysts, the COD removal rate was also different, with $Pt_{0.5}Cu_{1.5}$/AC-MR catalyst showing the best performance.

In general, the results shown in Fig. 7 shows that the performance of the Pt–Cu/AC-MR catalysts for aniline degradation was the best one among three cases of catalytic support. The good TOC removal ability was the same as good capability of mineralization rate of aniline (the efficiency of complete degradation to H_2O and CO_x) for the Pt–Cu/AC-MR catalysts. In contrast, the degradation of aniline by using the Pt–Cu/SiO_2 and Pt–Cu/Al_2O_3 catalysts was often not complete, and aniline may be degraded into other organic molecules which stayed in water. This is further supported by an interesting phenomenon described below.

As can be observed with naked eyes, the aniline solution was transparent almost during the entire degradation process when AC-supported catalysts were used. While SiO_2 was used as the catalytic support, the solution became brown quickly. Suspended black materials can be observed in the solution when Al_2O_3 was used. According to ref. 52, the oxidative degradation of aniline affords compounds in brown at the first stage, and then affords compounds in black, until it was completely degraded. This phenomenon further demonstrated that the choice of catalytic support was important, and the performances for degradation of aniline showed the order of AC > Al_2O_3 > SiO_2. This may be associable with different pore structures in different supports (Table 3), and the reduction method (see in Section 2.2) used affecting the dispersion of Pt and Cu components and generation of Pt, Cu and their alloys (see in Section 3.2).

3.3.3 Effect of metal loading and metal type. The results in Fig. 8 shows that the performance of different catalysts with a same support and a same overall metal loading followed the order of Pt–Cu/AC-MR > Pt–Fe/AC-MR > Cu/AC-MR > Pt/AC-MR. This order may be related to the possible synergistic effect between different metal components. At the same time, the performance of catalysts with different metal loadings was also different. However, during the experiment, the dissolution of the Fe component into water seemed to be serious, and therefore the subsequent studies using Fe catalysts did not continued. For the cases of Pt/AC-MR and Cu/AC-MR, the COD value was reduced to the lowest value within 1 h, and gradually increased in the following times, being still lower than the initial value, indicating that aniline was degraded to a certain degree.

The TOC removal rate was lower than the COD case, indicating that the degradation of aniline was incomplete and some other organic molecules were produced. For the supported monometallic catalysts, COD and TOC removal rate of the Cu/AC catalyst was higher than Pt/AC (Fig. 8b and c). First, the aniline molecules ma be physically adsorbed (*vide infra*) onto the outer surface of the catalyst and part of them may enter the inner pores, and then were degraded by the catalysis of the

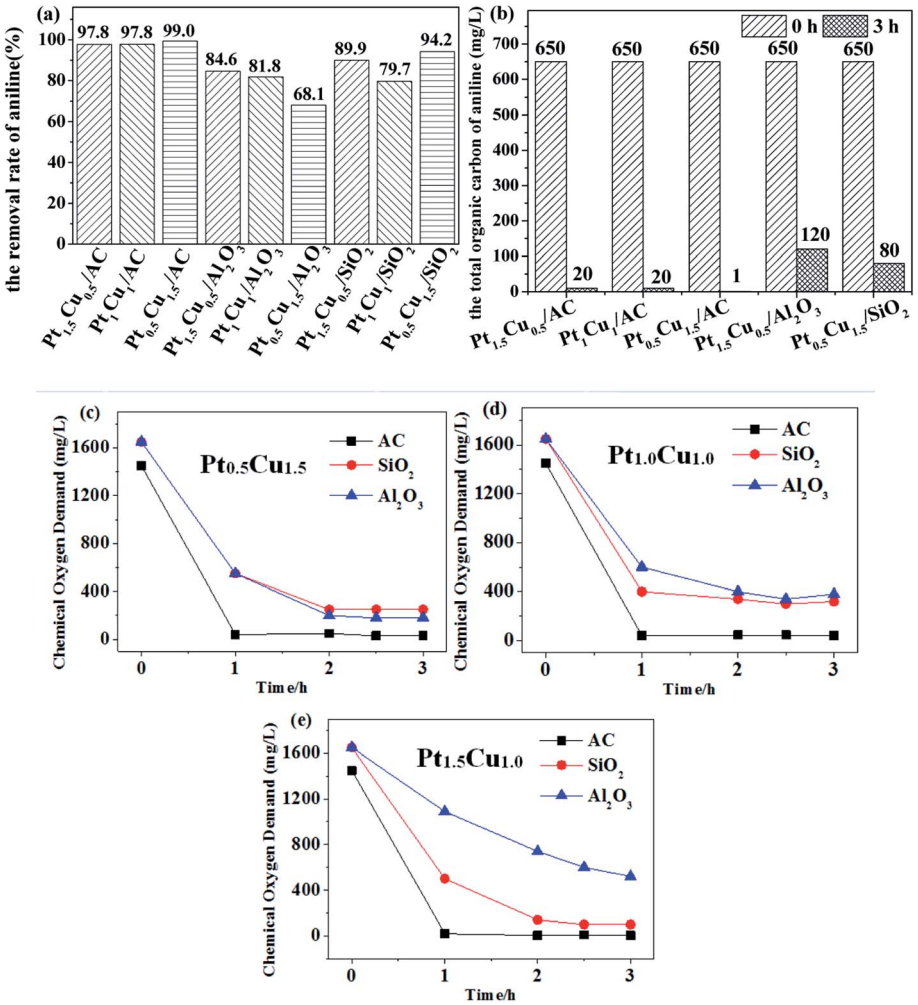

Fig. 7 The catalytic test results for different catalysts in terms of TOC or COD value of aniline at the presence of H_2O_2. (a) The TOC removal rate of aniline catalyzed by different catalysts as indicated, (b) the TOC value of catalytic degradation of aniline using different catalysts as indicated, (c) the COD value of catalytic degradation of aniline using $Pt_{0.5}Cu_{1.5}$/AC-MR, $Pt_{0.5}Cu_{1.5}/Al_2O_3$ and $Pt_{0.5}Cu_{1.5}/SiO_2$, respectively, as the catalysts (d) the COD value of catalytic degradation of aniline using $Pt_{1.0}Cu_{1.0}$/AC-MR, $Pt_{1.0}Cu_{1.0}/Al_2O_3$ and $Pt_{1.0}Cu_{1.0}/SiO_2$, respectively, as the catalysts (e) the COD value of catalytic degradation of aniline using $Pt_{1.5}Cu_{0.5}$/AC-MR, $Pt_{1.5}Cu_{0.5}/Al_2O_3$ and $Pt_{1.5}Cu_{0.5}/SiO_2$, respectively, as the catalysts. *Reaction conditions: H_2O_2 concentration = 0.098 mol L^{-1}, aniline concentration = 500 mg L^{-1}, dosage of catalyst = 5 g L^{-1}, temperature = 50 °C, and reaction time = 3 h.

active metal components, so the COD value decreased within 1 h. Then, the partly degraded products from aniline returned to the solution after a long time of stirring, leading to the COD value increased slightly again (Fig. 8). Comparison of the results shown in Fig. 8 with those in Fig. 7, it can be seen that the bimetallic Pt–Cu/AC-MR catalysts had a better performance for the catalytic removal of aniline than the monometallic Pt or Cu catalysts, although the overall metal loading were the same.

According to the definition of synergy effect in catalytic chemistry, the formula of synergy index (SI) can be expressed as follows.

$$\mathrm{SI} = \frac{K_{\mathrm{Pt-Cu/AC}}}{(1-x)K_{\mathrm{Cu/AC}} + xK_{\mathrm{Pt/AC}}}$$

Here x is $n/(m+n)$ for the Pt_nCu_m/AC-MR catalyst. According to the data of TOC removal rates in Fig. 7 and 8, the $SI_{(Pt-Cu)}$ was calculated to be 309–312%, which indicates that synergic effect on the Pt–Cu/AC-MR catalyst could improve the catalytic efficiency by up to 212% for the case of $Pt_{0.5}Cu_{1.5}$/AC-MR. So the synergistic effect of catalytic degradation of aniline was excellent. The possible reasons accounting for this effect may be associable with the dispersion of active components (Fig. 4) as well as the formation of alloy in the metal nanoparticles (see Fig. 2 and Table 2).

3.3.4 Preliminary discussion about the catalytic reaction mechanism of aniline degradation. In order to gain a deep understanding of the above catalytic/adsorption test results for Fenton oxidation of aniline in water, a simple catalytic reaction mechanism (see Scheme 1) was proposed according to the above results.

The pathways indicted with k_1–k_3 shown in Scheme 1 result in the oxidative degradation of aniline by reacting with H_2O_2.

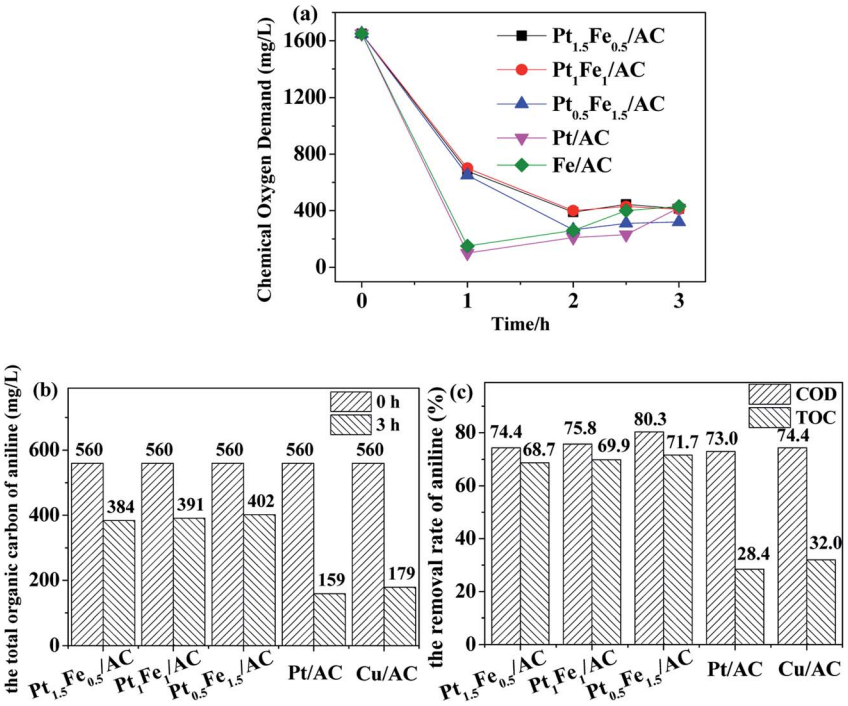

Fig. 8 The values of COD and TOC of the solution of Fenton oxidation of aniline using Pt–Cu/AC-MR, Cu/AC-MR, Pt/AC-MR, Pt–Fe/AC-MR as catalysts, respectively. (a) Effect of different catalysts on the COD value, (b) effect of different catalysts on TOC value, and (c) comparison of COD and TOC removals of each catalyst. *Reaction conditions: H_2O_2 concentration = 0.098 mol L^{-1}, aniline concentration = 500 mg L^{-1}, temperature = 50 °C, catalyst dosage = 5 g L^{-1}, degradation time = 3 h, overall metal loading = 2%.

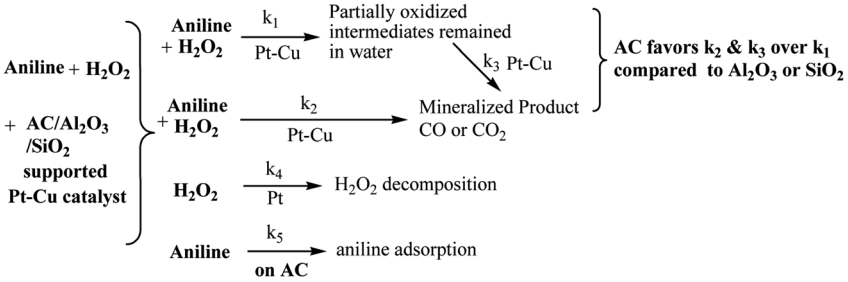

Scheme 1 Possible reaction mechanism of the reaction between aniline and H_2O_2 at the presence of supported bimetallic Pt–Cu catalysts.

However, not all aniline molecules can be directly oxidized to mineralized product of gaseous CO/CO_2, and part of the aniline intermediates remained in water, which is accounted for the difference of COD and TOC removal rates. From the catalytic test results shown in Fig. 7 and 8, it can be seen that the catalysts using AC as the support favors k_2 and/or k_3 over k_1 compared to the ones using Al_2O_3 or SiO_2 as supports. The contribution of the physical adsorption processes (k_5) should be further noted during the catalytic degradation of aniline with the involvement of AC, as reflected by the results shown in Fig. 8a. Competing with pathways k_1–k_3, pure catalytic decomposition of H_2O_2 also occurred. As is known, decomposition of H_2O_2 to produce reactive intermediate of HO˙radical is key to oxidize aniline, however, not all reactive intermediate can attack aniline or its intermediate, leading to a pure decomposition process. An increasing amount of Pt was advantageous to the H_2O_2 decomposition (Fig. 6), however, too much Pt component may lead to a larger portion of H_2O_2 decomposition. A good catalyst should be able to give large k_4 and at the same time give large $(k_1 + k_3)/k_4$. From this point of view, the significant synergic effect of the $Pt_{0.5}Cu_{1.5}$/AC-MR catalyst may be accounted for its ability to accelerate the rate of H_2O_2 decomposition (k_4), and the rate of aniline oxidation (k_1–k_3, in particular, k_1 and k_3) at the same time, with the preference of the latter pathways. A detailed mechanism study of the related catalytic systems are undergoing in our group.

3.3.5 Comparison of the result of this work with other works in the literature. When the reaction time was shortened from 3 h (Fig. 7) to 1 h (Fig. 9), it can been seen that the COD value did not change after 1 h, and the decomposition of H_2O_2 almost stopped at 30 min. These phenomena showed that aniline could be almost completely degraded in 1 h at 50 °C.

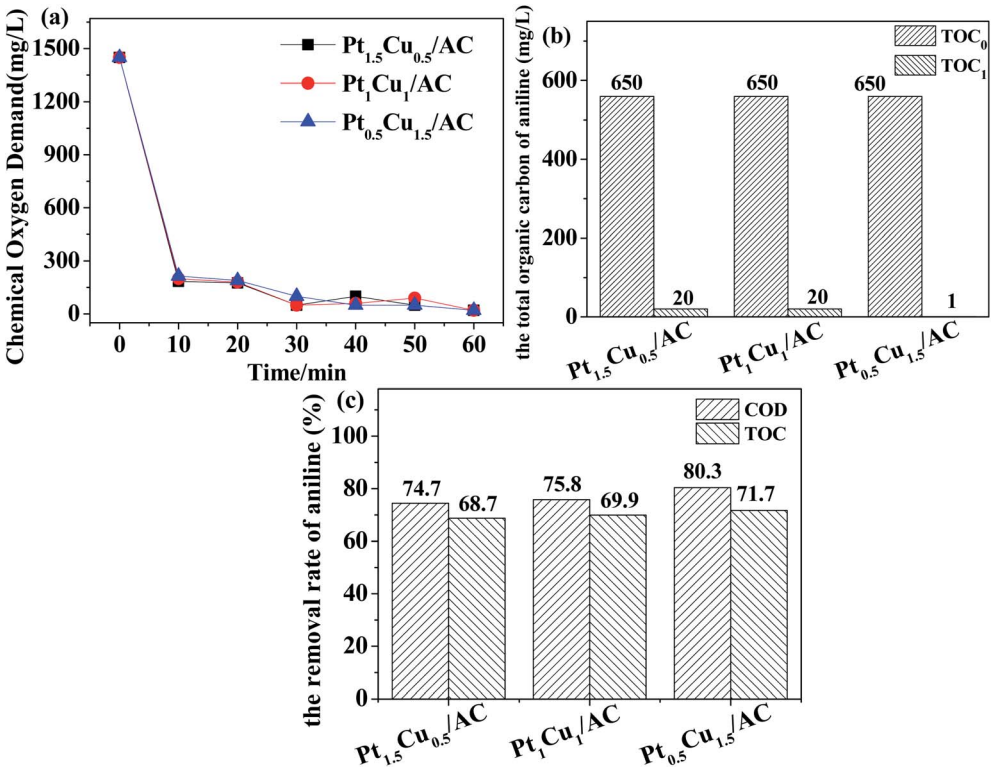

Fig. 9 The effect of different metal loadings on catalytic degradation of aniline by using Pt–Cu/AC-MR. (a) The COD value of the solution, (b) the TOC value of the solution, (c) the COD and TOC removal rate after 1 h. *Reaction conditions: H_2O_2 concentration = 0.098 mol L^{-1}, aniline concentration = 500 mg L^{-1}, the catalyst dosage = 5 g L^{-1}, degradation reaction time = 1 h, overall metal loading capacity = 2% and reaction temperature = 50 °C.

Table 4 Comparison of the catalytic performance of our catalysts to those in the similar works in the literature for oxidative degradation of aniline in water

Catalyst	TOC or COD removal	Conditions	References
$Pt_{0.5}Cu_{1.5}$/AC-MR	Up to 99% TOC removal	50 °C, 5 g L^{-1} catalyst, 500 mg L^{-1} aniline, 0.098 mol L^{-1} H_2O_2, 60 min	This work
5% Ru/SiO_2	90% COD	200–220 °C, 0.69 MPa O_2, 1.33 g L^{-1} catalyst, 500 ppm aniline, 120 min	53
$Ru/Ti_{0.9}Zr_{0.1}O_2$	84.6% COD	180 °C, 1.5 MPa O_2, 4 g L^{-1} catalyst, 2 g L^{-1} aniline, 300 min	54
PAC@$Fe^{II}Fe_2^{III}O_4$	71.2% aniline	25 °C, pH = 6, UV + 5 mmol $L^{-1}H_2O_2$, 0.3 g L^{-1} catalyst, 120 mg L^{-1} aniline, 180 min	55
10 mg L^{-1} Fe^{2+}	78% COD	25 °C, pH = 8, 2.08 mg min^{-1} $L^{-1}O_3$, 10 mg L^{-1} catalyst, 75 mg L^{-1} AAF, 180 min	56
Co/Fe(3 : 1)-LDH	88% COD	70 °C, pH = 12, 400 mL min^{-1} O_3, 12.5 g L^{-1} catalyst, 960 mg L^{-1} initial COD, 180 min	57

And $Pt_{0.5}Cu_{1.5}$/AC-MR had best performance on degradation and mineralization, and removal of TOC was more than 99%. The reason for this phenomenon was that the slightly higher loading of Pt has high catalytic activity, and the hydrogen peroxide is rapidly decomposed on the catalyst surface, which affects the further oxidative degradation of the migration of aniline molecules to the inner surface of PtCu/AC-MR. A summary of comparison of the results of our work with other similar works can be seen in Table 4, which showed the superiority of our catalytic systems for oxidative degradation of aniline in water. It is interesting to notice that in our catalytic systems, the pH value of the solution did not required to adjust to a typical case of 3–4 in many Fenton reaction researches, and instead, the solutions were almost neutral in this work. This adds to the appealing advantage of our catalysts for potential application in the Fenton oxidation of aniline in particular and of organic pollution in general.

4. Conclusion

This paper reports a systematic investigation of the supported Pt–Cu bimetallic catalysts prepared with various impregnation methods, and their performances for catalytic Fenton oxidation of aniline in water as well. Various preparation conditions including impregnation amount, bimetallic type, impregnation ratio of two metals, reduction temperature, reduction method, and types of catalytic support were changed to obtain different supported catalysts. In particular, the methanal reduction (MR) method developed in this work was reported for the first time to the best of our knowledge.

The XRF analysis results revealed that the MR method led to more metal lost on Pt–Cu/AC than the H_2 reduction method, but the particle diameter was rather small (concentrated in the <3 nm range, by TEM) for the former case. The XRD analysis results disclosed that Pt–Cu alloy can be formed in the bimetallic catalysts. However, the crystal phase of AC was destroyed the specific surface area and was decreased significantly, and the pore volume was slightly increased. The results of BET show that the specific surface area of the catalyst supported on AC was significantly larger than that of Al_2O_3 and SiO_2.

$Pt_{0.5}Cu_{1.5}$/AC-MR presented the highest activity for catalytic degradation of aniline (500 mg L^{-1}) in the neutral aqueous solution among all catalysts examined. The catalytic test results showed that the liquid pollutant was almost completely degraded within 60 minutes at the presence of 0.098 mol L^{-1} H_2O_2 using this catalyst. The performance of $Pt_{0.5}Cu_{1.5}$/AC-MR was much better than Pt/AC and Cu/AC under the same preparation and reaction conditions, which showed that there was a significant synergic effect between the Pt and Cu components. The synergic effect may lead to an improvement of catalytic efficiency by 212% in this case in terms of TOC removal rate. This effect could play a pivotal role for the degradation of aniline and also provide potential hopefulness for future industrial application.

Author contributions

Qiuyue Ding: catalyst preparation, characterization, reaction test, writing. Wumin Zhang: catalyst preparation, reaction test, analysis, writing. Yuanyuan Zhu: catalyst preparation, characterization. Lu Wang: catalyst preparation, reaction test. Yanyan Xi: catalyst preparation, characterization, discussion. Xufeng Lin: idea development, research funding provision, writing and organization. Xiyuan Feng: catalyst preparation, reaction setup construction.

Conflicts of interest

There are no conflicts to declare.

Acknowledgements

Support from the National Natural Science Foundation of China (21576291), and Shandong Province Natural Science Foundation (ZR2014BM002) is gratefully acknowledged.

References

1 S. Shi, J. Cao, L. Feng, W. Liang and L. Zhang, *Chin. J. Environ. Eng.*, 2015, **9**, 4871–4876.
2 S. Jiang, J. Zhu, S. Bai, Y. Guan and J. Yao, *Desalin. Water Treat.*, 2016, **57**, 791–798.
3 J. Xiang, Z. Zhang, H. Fan and S. Lv, *Environ. Sci. Technol.*, 2010, **33**, 81–85.
4 S. Vimalnath, H. Ravishankar, C. Schwandt, R. V. Kumar and S. Subramanian, *Water Sci. Technol.*, 2018, **78**, 290–300.
5 W. W. Eckenfelder, *Stud. Environ. Sci.*, 1986, **29**, 43–50.
6 B. Wang, X. Wu, Y. Luo and Y. Liu, *Ind. Water Treat.*, 2015, **35**, 93–95.
7 M. Kiel, D. Dobslaw and K. H. Engesser, *Water Res.*, 2014, **66**, 1–11.
8 C. Comninellis, *Electrochim. Acta*, 1994, **39**, 1857–1862.
9 X. Nie, T. Huang, J. Zhang, S. Zhang, H. Chen, L. Ding and L. Liu, *Huanjing Kexue*, 2012, **32**, 274–278.
10 J. Yoon, Y. Lee and S. Kim, *Water Sci. Technol.*, 2001, **44**, 15–21.
11 W. Z. Tang and C. P. Huang, *Environ. Technol.*, 1996, **17**, 1371–1378.
12 W. Y. Zhao, X. F. Zheng, L. W. Xu and G. Y. Yang, *Adv. Mat. Res.*, 2013, **726**, 1710–1714.
13 Z. Y. Li, W. Song and L. Zhang, *Adv. Mat. Res.*, 2013, **781**, 2184–2188.
14 Y. H. Huang, Y. F. Huang, P. S. Chang and C. Y. Chen, *J. Hazard. Mater.*, 2008, **154**, 655–662.
15 Y. Jing and B. P. Chaplin, *Environ. Sci. Technol.*, 2017, **51**, 2355–2365.
16 C. Lee, J. Yoon and U. V. Gunten, *Water Res.*, 2007, **41**, 581–590.
17 N. A. Landsman, K. L. Swancutt, C. N. Bradford, C. R. Cox, J. J. Kiddle and S. P. Mezyk, *Environ. Sci. Technol.*, 2007, **41**, 5818–5823.
18 S. A. Wang, *Dyes Pigm.*, 2008, **76**, 714–720.
19 F. Velichkova, H. Delmas, C. Julcour and B. Koumanova, *AIChE J.*, 2017, **63**, 669–679.
20 J. J. Pignatello, *Environ. Sci. Technol.*, 1992, **26**, 944–951.
21 J. Sun, X. Li, J. Feng and X. Tian, *Water Res.*, 2009, **43**, 4363–4369.
22 S. T. Yang, W. Zhang, J. Xie, R. Liao, X. Zhang, B. Yu, R. Wu, X. Liu, H. Li and Z. Guo, *RSC Adv.*, 2015, **5**, 5458–5463.
23 S. T. Christensen, H. Feng, J. L. Libera, N. Guo, J. T. Miller, P. C. Stair and J. W. Elam, *Nano Lett.*, 2010, **10**, 3047–3051.
24 Y. H. Huang, C. C. Su, Y. P. Yang and M. C. Lu, *Environ. Prog. Sustain. Energy*, 2013, **32**, 187–192.
25 J. Choi, J. H. Jeong and J. Chung, *Chem. Eng. J.*, 2013, **218**, 260–266.
26 Z. Huang, Z. Chen, Y. Chen and Y. Hu, *Chemosphere*, 2018, **203**, 442–449.
27 Z. Han, Y. Dong and S. Dong, *J. Hazard. Mater.*, 2011, **189**, 241–248.
28 I. Yamanaka and Y. Nabae, *Adv. Sci. Technol.*, 2006, **45**, 2067–2076.

29 A. Ciftci, M. D. A. J. Ligthart, O. A. Sen, V. A. J. F. Hoof, H. Friedrich and E. J. M. Hensen, *J. Catal.*, 2014, **311**, 88–101.
30 Y. Liu, G. Zhang, S. Fang, S. Chong and J. Zhu, *J. Environ. Manage.*, 2016, **182**, 367–373.
31 C. Vidya, C. Manjunatha, M. N. Chandraprabha, M. Rajshekar and M. A. L. A. Raj, *J. Environ. Chem. Eng.*, 2017, **5**, 3172–3180.
32 Y. S. González, C. Costa, M. C. Márquez and P. Ramos, *J. Hazard. Mater.*, 2011, **187**, 101–112.
33 J. D. Zeeuw, D. R. C. M. Nijs and L. T. Henrich, *J. Chromatogr. Sci.*, 1987, **25**, 71–83.
34 Y. Xie, Y. Zhu, B. Zhao and Y. Tang, *Stud. Surf. Sci. Catal.*, 1998, **118**, 441–449.
35 M. Ciobanu, G. Petcu, E. M. Anghel, F. Papa, N. G. Apostol, D. C. Culita, I. Atkinson, S. Todorova, M. Shopska, A. Naydenov, R. Velinova and V. Parvulescu, *Appl. Catal., A*, 2021, **619**, 118123.
36 M. Zhang, S. Cai, J. Li, E. A. Elimian, J. Chen and H. Jia, *J. Hazard. Mater.*, 2021, **412**, 125266.
37 Y. Zhou, D. Liu, W. Qiao, Z. Liu, J. Yang and L. Feng, *Materials Today Physics*, 2021, **17**, 100357.
38 Z. Lan, Y. Yu, H. Li, L. Zhang and Y. Cao, *Mater. Sci. Semicond. Process.*, 2021, **123**, 105547.
39 Y. Xi, J. Xiao, X. Lin, W. Yan, C. Wang and C. Liu, *Ind. Eng. Chem. Res.*, 2018, **57**, 10137–10147.
40 X. Li, X. You, P. Ying, J. Xiao and C. Li, *Top. Catal.*, 2003, **25**, 63–70.
41 C. E. Huckaba and F. G. Keyes, *J. Am. Chem. Soc.*, 1948, **70**, 1640–1644.
42 P. Shafiee, S. M. Alavi and M. Rezaei, *J. Energy Inst.*, 2021, **96**, 1–10.
43 N. Ji, Z. Liu, X. Diao, J. Bao, Z. Yu, C. Song, Q. Liu, D. Ma and X. Lu, *Mol. Catal.*, 2020, **495**, 111155–111163.
44 A. H. Valekar, K. R. Oh, S. K. Lee and Y. K. Hwang, *J. Ind. Eng. Chem.*, 2021, **101**, 66–77.
45 H. Lee, W. I. Kim, K. D. Jung and H. L. Koh, *Korean J. Chem. Eng.*, 2017, **34**, 1337–1345.
46 X. Zhang, N. He, C. Liu and H. Guo, *Catal. Letters*, 2019, **149**, 974–984.
47 W. Wang, K. Nakagawa, T. Yoshikawa, T. Masuda, E. Fumoto, Y. Koyama, T. Tago and H. Fujitsuka, *Appl. Catal. A Gen.*, 2021, **619**, 118152–118160.
48 M. H. Stacey, *Stud. Surf. Sci. Catal.*, 1988, **39**, 55–65.
49 A. V. Neimark, *Stud. Surf. Sci. Catal.*, 1991, **62**, 67–74.
50 S. S. Lin and M. D. Gurol, *Water Sci. Technol.*, 1996, **34**, 57–64.
51 G. T. Chi and K. D. Huddersman, *J. Adv. Oxid. Technol.*, 2011, **14**, 235–243.
52 M. Martinez, A. Irabien, A. R. Arnaiz and C. Santiago, *J. Therm. Anal. Calorim.*, 1984, **29**, 251–255.
53 G. R. Reddy and V. V. Mahajani, *Ind. Eng. Chem. Res.*, 2005, **44**, 7320–7328.
54 M. Song, Y. Wang, Y. Guo, L. Wang, W. Zhan, Y. Guo and G. Lu, *Chin. J. Catal.*, 2017, **38**, 1155–1165.
55 M. Ahmadi, B. Kakavandi, S. Jorfi and M. Azizi, *J. Photochem. Photobiol.*, 2017, **336**, 42–53.
56 P. Fu, L. Wang, G. Li, Z. Hou and Y. Ma, *J. Environ. Chem. Eng.*, 2020, **8**, 103714–103721.
57 Y. Qi, C. Guo, X. Xu, B. Gao, Q. Yue, B. Jiang, Z. Qian, C. Wang and Y. Zhang, *Sci. Total Environ.*, 2020, **715**, 136982–136994.